Physics and Chemistry of the Earth 131 (2023) 103451

Contents lists available at ScienceDirect

Physics and Chemistry of the Earth

journal homepage: www.elsevier.com/locate/pce

An improved adaptive neuro-fuzzy inference system for hydrological drought prediction in Algeria

Mohammed Achite [a,b], Enes Gul [c], Nehal Elshaboury [d], Muhammad Jehanzaib [e,f], Babak Mohammadi [g,*], Ali Danandeh Mehr [h,i]

[a] Laboratory of Water and Environment, Faculty of Nature and Life Sciences, Hassiba Benbouali University of Chlef, Chlef, 02180, Algeria
[b] Georessources, Environment and Natural Risks Laboratory, University of Oran, Oran, 31000, Algeria
[c] Department of Civil Engineering, Inonu University, 44280, Malatya, Turkey
[d] Construction and Project Management Research Institute, Housing and Building National Research Centre, Giza, 12311, Egypt
[e] Research Institute of Engineering and Technology, Hanyang University, Ansan, 15588, Republic of Korea
[f] Department of Civil Engineering & Technology, Qurtuba University of Science and Information Tecnology, Dera Ismail Khan, 29050, Pakistan
[g] Department of Physical Geography and Ecosystem Science, Lund University, Sölvegatan 12, SE 223 62, Lund, Sweden
[h] Civil Engineering Department, Antalya Bilim University, Antalya, 07190, Turkey
[i] MEU Research Unit, Middle East University, Amman, 11831, Jordan

ARTICLE INFO

Keywords:
Hydrological drought
Hybrid model
ANFIS
Water cycle algorithm: semi-arid regions

ABSTRACT

Drought has negative impacts on water resources, food security, soil degradation, desertification and agricultural productivity. The meteorological and hydrological droughts prediction using standardized precipitation/runoff indices (SPI/SRI) is crucial for effective water resource management. In this study, we suggest ANFISWCA, an adaptive neuro-fuzzy inference system (ANFIS) optimized by the water cycle algorithm (WCA), for hydrological drought forecasting in semi-arid regions of Algeria. The new model was used to predict SRI at 3-, 6-, 9-, and 12-month accumulation periods in the Wadi Mina basin, Algeria. The results of the model were assessed using four criteria; determination coefficient, mean absolute error, variance accounted for, and root mean square error, and compared with those of the standalone ANFIS model. The findings suggested that throughout the testing phase at all the sub-basins, the proposed hybrid model outperformed the conventional model for estimating drought. This study indicated that the WCA algorithm enhanced the ANFIS model's drought forecasting accuracy. The proposed model could be employed for forecasting drought at multi-timescales, deciding on remedial strategies for dealing with drought at study stations, and aiding in sustainable water resources management.

1. Introduction

Deficiency of precipitation is referred as drought that disrupts the natural life process for humans, crops, and animals (Zargar et al., 2011). It has serious consequences for water supplies and use in drinking and irrigation, crop yields, increasing the risk of wildfires, and shortage of water for hydropower (Belayneh et al., 2016; Danandeh Mehr et al., 2020; Hanjra and Qureshi, 2010; Hao et al., 2014). Drought is frequently forecasted at monthly or seasonal timeframes utilizing various climatic factors (Hao et al., 2018). Nonetheless, due to its complexity, gradual occurrence, and various causative elements at distinct temporal and geographical extend, drought remains one of the most poorly understood natural events (Adnan et al., 2021a). An explanation of the drought types and indicators is required for better understanding of this phenomenon.

Droughts are grouped into four types based on their duration (Ahmadalipour et al., 2017; Mehran et al., 2015): hydrologic, meteorological, socioeconomic, and agricultural droughts. For hydrologic drought, identifying parameters such as a lack of groundwater supplies or streamflow shortages is required; for meteorological drought, identifying variables such as transpiration, evaporation, and precipitation is required (Li et al., 2020, 2021). Also, information on water storage resilience and inflow-demand reliability are needed for socioeconomic drought. Finally, for agricultural drought, identifying parameters such as evaporation stress and soil moisture deficit is required. A variety of drought indicators have been suggested to assess the severity of

* Corresponding author.
E-mail addresses: m.achite@univ-chlef.dz (M. Achite), enes.gul@inonu.edu.tr (E. Gul), nehal.elshabory@hbrc.edu.eg (N. Elshaboury), jehanzaib7@hanyang.ac.kr (M. Jehanzaib), babak.mohammadi@nateko.lu.se (B. Mohammadi), ali.danandeh@antalya.edu.tr (A. Danandeh Mehr).

https://doi.org/10.1016/j.pce.2023.103451
Received 28 February 2023; Received in revised form 30 April 2023; Accepted 26 July 2023
Available online 31 July 2023

droughts. The Palmer drought severity index (PDSI) (Palmer, 1965), drought area index (DAI) (Bhalme and Mooley, 1980), standardized precipitation index (SPI) (Mckee et al., 1993) and standardized precipitation evapotranspiration index (SPEI) (Vicente-Serrano et al., 2010) are just a few examples of meteorological drought indices. It is worth mentioning that DAI and SPI are calculated using historical precipitation data, whereas SPEI and PDSI require temperature as well. These indexes are widely utilized to aid decision-makers in the implementation of efficient drought mitigation and adaptation strategies (AghaKouchak, 2014; Hosseini-Moghari and Araghinejad, 2015; Ribeiro and Pires, 2016).

In recent decades, different types of machine learning algorithm such as artificial neural networks (Doshi et al., 2022; Pande et al., 2022), support vector machine (Emamgholizadeh and Mohammadi, 2021), and various kind of optimization algorithms such as genetic algorithm (A.K. Singh et al., 2022) and grey wolf optimizer (Mirboluki et al., 2022), have been successfully applied to environmental studies (Ham et al., 2022; Panda et al., 2022; V.K. Singh et al., 2022). Many studies have been recently published to anticipate drought indicators by utilizing machine learning models (e.g., Belayneh et al., 2016; Gholizadeh et al., 2022; Mehdizadeh et al., 2020; Mohammadi, 2023). For instance, Malik et al. (2020) applied the co-active neuro-fuzzy inference system for forecasting the SPI based on drought data in Uttarakhand, India. The model was compared to a multilayer perceptron and multiple linear regression using performance metrics and graphical representations. The developed model outscored the other models, with varying outcomes depending on the meteorological station. Sattar et al. (2020) used the Markov Bayesian classifier model to assess the hydrological and meteorological drought, as defined by the SPI and standardized runoff index (SRI), respectively. The model's accuracy in forecasting meteorological drought ranged from 36% to 76%, while its accuracy in predicting hydrological drought ranged from 33% to 70%.

Başakın et al. (2021) forecasted the self-calibrated PDSI (sc-PDSI) using the adaptive neuro-fuzzy inference system (ANFIS). For ANFIS, Nash-Sutcliffe efficiency (NSE) = 0.52 and 0.17 for 3 and 6 months, respectively compared to 0.81 and 0.77 for the hybrid model. Therefore, the hybrid model outperformed the standalone ANFIS model for drought prediction in Adana, Turkey. Danandeh Mehr et al. (2021) employed the multi-temporal SPEI to measure drought at two meteorological stations in Ankara, Turkey. The conventional genetic programming (GP) was used to formulate the deterministic sub-signal. The novel model was cross-validated against the GP, random forest, and first-order autoregressive models.

Jehanzaib et al. (2021) predicted hydrological drought in the Han River basin, South Korea by accounting for humidity, temperature, and precipitation. With an average root mean square error (RMSE) of 0.34, NSE of 0.87, mean absolute error (MAE) of 0.26, and determination coefficient (R^2) of 0.89, the decision tree (DT) approach exhibited the best performance in all watersheds. Achite et al. (2022b) compared various artificial intelligence models for hydrological drought prediction in the Wadi Ouahrane Basin (WOB), Algeria. The ANFIS, DT, artificial neural network (ANN), and support vector machine (SVM) models were developed and evaluated. According to the outcomes, the SVM approach outperformed the other models, with an average MAE of 0.19, R^2 of 0.90, RMSE of 0.28, and NSE of 0.86.

The development of machine learning models for tackling various engineering issues has progressed dramatically during the last two decades. The speed and flexibility of data analysis distinguish machine learning models from traditional time-series models. Moreover, these models may use training data to establish the correlation between input and output variables (Liang et al., 2021). However, constraints on feature extraction, human interaction, internal parameter adjustment, and other topics have been reported (Yaseen et al., 2015, 2018). The ANN model, for example, has the disadvantage of trapping in local minima, necessitating the application of an optimization method (Jadav and Panchal, 2012).

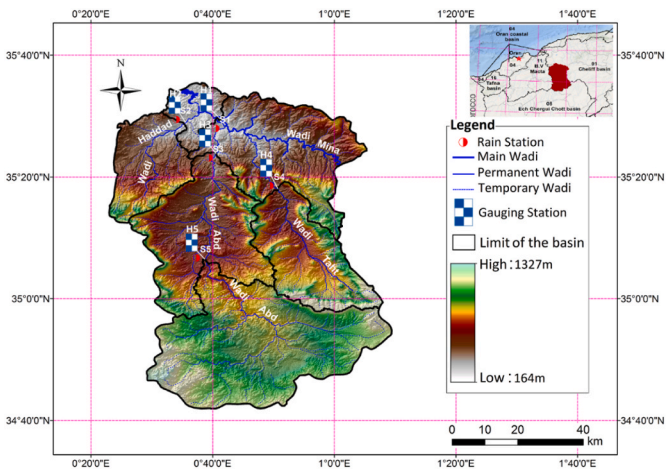

Fig. 1. Map of the study area along with location of hydro-meteorological stations.

To enhance the predictive performance of models, machine learning models were coupled with optimization algorithms. Adnan et al. (2021b) combined the random vector functional link (RVFL) with the salp swarm algorithm (SSA), particle swarm optimization (PSO), hunger games search (HGS), grey wolf optimization, genetic algorithm, and social spider optimization to forecast droughts using the monthly precipitation data from three Bangladeshi stations. The HGS algorithm outperformed the other algorithms, significantly improving the accuracy of the RVFL method in drought forecasting. Achite et al. (2022a) applied the Bayesian model averaging (BMA) with ANNs to forecast SPI indices. The models included optimized ANN using PSO, SSA, water strider algorithm (WSA), and sine cosine algorithm. For SPI-6 and SPI-12 forecasts, the most accurate models were ANN combined with BMA and WSA. The optimization algorithms improved the drought forecasting accuracy of ANN models. However, hybrid machine learning's applicability has yet to be thoroughly investigated in the hydrological field, particularly in drought modeling. The novelty of this study is to propose a hybrid framework to improve the efficiency of traditional ANFIS model using advanced optimization algorithm which has not done so far. Therefore, this study employed ANFIS model that is optimized using the water cycle optimization (WCA) algorithm, namely ANFISWCA, for hydrological drought forecasting in Wadi Mina, Algeria. The fundamental concepts and ideas which underlie the WCA are inspired by nature and based on the observation of water cycle process and how rivers and streams flow into to the sea (Sadollah et al., 2016). Moreover, the optimization concept of WCA algorithm fits good in water resources problems.

The problem of water scarcity brought on by the significant temporal and spatial variability of precipitation is ubiquitous in arid and semi-arid countries including Algeria. The frequency of drought occurrences increased in Algeria, having a devastating influence on local water supplies and agriculture (Habibi et al., 2018; Rahmouni et al., 2022). As such, it is critical to develop drought prediction systems to provide early warning and timely implementation of mitigation and adaptation measures (Azizi et al., 2019; Moreira et al., 2008). Therefore, the major objectives of this research are: 1) investigating a hybrid approach (ANFISWCA) that combines the adaptive neuro-fuzzy inference system with the water cycle algorithm to predict hydrological drought in Algeria. The use of a hybrid approach could be a novel contribution, as it combines the strengths of different methods to improve accuracy and robustness. The WCA was examined for training ANFIS because of its promising performance in offering the best solutions in many domains (Rais et al., 2022; Yadav and Verma, 2020). 2) Appling the proposed approach to a specific case study of hydrological drought prediction in Algeria. This application could be a novel contribution, as it

Table 1
Description of studied sites.

ID		Name	Elevation (m)	Latitude	Longitude
S1	013306	Oued Abtal	354	35°28′03.59" N	0°40′33.97" E
S2	013401	Sidi Abdelkader Djillali	225	35°29′20.71" N	0°34′08.35" E
S3	013302	Ain Hammara	288	35°23′15.39" N	0°39′16.85" E
S4	013001	Kef Mehboula	475	35°18′40.72" N	0°49′34.20" E
S5	013304	Takhmaret	655	35°06′49.01" N	0°37′27.25" E

demonstrates the effectiveness of the proposed approach in a real-world scenario and provides insights for future research on hydrological drought prediction in Algeria. The proposed model can be used to develop a robust system for predicting hydrological drought across several timelines and deciding on drought remediation solutions at study stations, as well as assisting in sustainable water resources management.

2. Study region

The Wadi Mina basin which is located between 34°41′57" N and 35° 35′ 27" N and between 00° 22′ 59" E to 01° 09′ 02" E in northwest Algeria was selected as the case study in this research (Fig. 1). Its altitude varies from 164 to 1327 m, with an area of 4900 km^2. It has a complex and rugged topography and continental climate with substantial temperature variations. For the ground vegetation cover, scrubs account for 32% as well as forests and cereal crops account for 35.8%. The mean of annual temperature ranges from 16 to 19.5 °C. The yearly precipitation averages 500 to 250 mm, with the majority of that falling between November and March (Achite and Touaibia, 2007). In this study, monthly data of rainfall and runoff was obtained for five hydro-meteorological stations during the period 1974 to 2009 (Tables 1-2 and Fig. 1).

3. Methodology

3.1. Standardized precipitation/runoff indices (SPI/SRI)

Two studied drought indices (namely SPI and SRI) were calculated using the accumulative likelihood of monthly precipitation and runoff, respectively (Awange et al., 2016). In the case of SPI, gamma probability distribution was fitted to long-term cumulative precipitation time series using Eq. (1).

$$g(x) = \frac{1}{\beta^{\alpha}\Gamma(\alpha)} x^{\alpha-1} e^{-x/\beta} \tag{1}$$

where, β and α stands for scale and shape components, respectively. While x represents cumulated precipitation and gamma function $\Gamma(\alpha)$ is determined by Eq. (2).

$$\Gamma(a) = \int_0^{\infty} y^{a-1} e^{-y} dy \tag{2}$$

The scale and shape parameters are determined using the precipitation time series as per Eq. (3).

$$\alpha = \frac{1}{4A}\left(1 + \sqrt{1 + \frac{4A}{3}}\right), A = ln(\overline{x}) - \frac{\sum \ln(x_i)}{n}, \beta = \frac{\overline{x}}{\alpha} \tag{3}$$

where, $\overline{x}$ and x_i refer to the average and total precipitations, respectively. Meanwhile, n is the number of data points. Equations (4) and (5) can be used to illustrate the cumulative probability.

$$G(x) = \int_0^x g(x)dx = \frac{1}{\beta^{a}\Gamma(a)} \int_0^x x^{a-1} e^{-x/\beta} dx \tag{4}$$

$$H(x) = q + (1-q)G(x) \tag{5}$$

Where, q is the probability of zero precipitation. Eq. (6) (Naresh Kumar et al., 2009) uses for the SPI calculation as follows.

$$SPI = \begin{cases} -\left(t - \dfrac{c_0 + c_1 t + c_2 t^2}{1 + d_1 t + d_2 t^2 + d_3 t^3}\right), 0 < H(x) \le 0.5 \\ +\left(t - \dfrac{c_0 + c_1 t + c_2 t^2}{1 + d_1 t + d_2 t^2 + d_3 t^3}\right), 0.5 < H(x) \le 1.0 \end{cases} \tag{6}$$

Where c_n and d_n are coefficients and t is defined by Equation (7).

$$t = \begin{cases} \sqrt{ln\left(\dfrac{1}{H(x)^2}\right)}. 0 < H(x) \le 0.5 \\ \sqrt{ln\left(\dfrac{1}{(1-H(x))^2}\right)}. 0.5 < H(x) \le 1.0 \end{cases} \tag{7}$$

Also, SPI can be used to explore various categorizes of wet and dry classes for the period under consideration (see Table 3) (Mckee et al., 1993). Similarly, for SRI, the hydrometric data was fitted to log-normal probability distribution, and accumulative probabilities were then converted into a standard normal variate using Eqs. (5)–(7).

3.2. Overview of ANFIS

ANFIS refers to a combined ANN and fuzzy logic (FL) simulation

Table 3
Categorization of SPI/SRI drought indices.

SPI/SRI values	Drought category	Probability (%)
≥2.00	Extremely wet	2.3
1.50–1.99	Very wet	4.4
1.00–1.49	Moderate wet	9.2
−0.99–0.99	Near normal	68.2
−1.00–−1.49	Moderately drought	9.2
−1.50–−1.99	Severely drought	4.4
≤ −2.00	Extremely drought	2.3

Table 2
Characteristics of gauging stations.

ID		Name	Elevation (m)	Basin area (km^2)	Latitude	Longitude
H1	013402	Oued Abtal	210	4126	35°29′26.28" N	0°41′00.49" E
H2	013401	Sidi Abdelkader Djillali	241	480	35°28′46.05" N	0°35′19.99" E
H3	013302	Ain Hammara	285	2480	35°23′50.09" N	0°40′33.19" E
H4	013001	Kef Mehboula	502	680	35°18′05.21" N	0°50′47.89" E
H5	013301	Takhmaret	634	1553	35°06′20.08" N	0°38′46.54" E

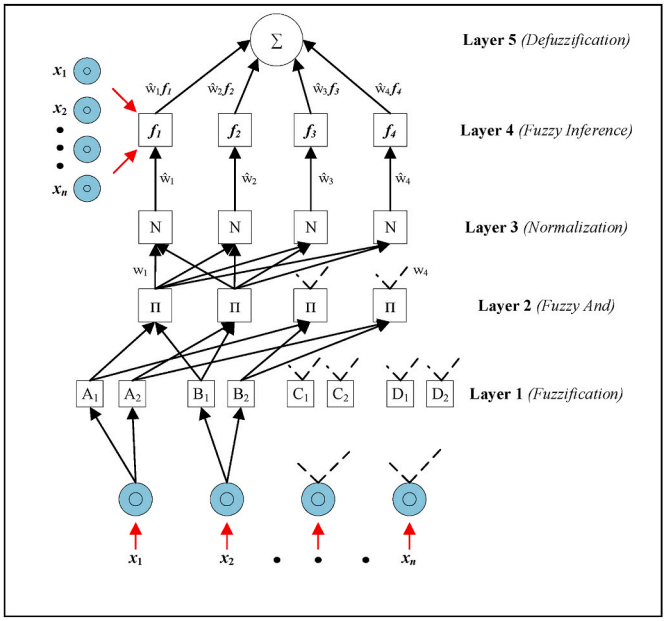

Fig. 2. The graphical representation of the ANFIS structure.

approach. This model was designed to overcome the FL and ANN deficiencies. Nevertheless, the basic knowledge of the set of constraints inspired by fuzzy structures indicates a reduction in the search area of optimization. Meantime, ANN backpropagation enables a coordinated network. ANN determines membership functions (MFs) used in this process (Singh et al., 2012). The rule base consists of Sugeno-type rules. The typical rule with four inputs, two fuzzy rules, and one output variable in this model is:

$$Rule\ 1: if\ C_v\ is\ A_1, D_{gr}\ is\ B_1, \begin{matrix}(d/R)\ is\ C_1\ and\ \lambda\ is\ D_1\ then\ f_1\\ = p_1C_v + q_1D_{gr} + r_1(d/R) + s_1\lambda + u_1\end{matrix}$$

$$Rule\ 2: if\ C_v\ is\ A_2, D_{gr}\ is\ B_2, \begin{matrix}(d/R)\ is\ C_2\ and\ \lambda\ is\ D_2\ then\ f_2\\ = p_2C_v + q_2D_{gr} + r_2(d/R) + s_2\lambda + u_2\end{matrix}$$

Where, p, q, r, s, and u are parameters that are determined by ANNs.

The first layer of the five-layered structure of ANFIS is fuzzification (Fig. 2): input values are converted to fuzzy sets. Membership functions (MFs) are used to fuzzify data, with the Gaussian, trapezoidal, triangular, and bell functions being the most prevalent. The bell function was selected in this study because it is concise and has a smooth notation:

$$O_i^1 = \mu_{A_i}(x) \quad i = 1,2 \tag{8}$$

$$\mu_{A_i}(x) = \frac{1}{1 + \left\{\left(\frac{x-c_i}{a_i}\right)^2\right\}^{b_i}} \tag{9}$$

Where, O is the layer output, $\mu_{A_i}(x)$ is the bell function, a_i, b_i, c_i are the premise parameters of the bell function (Jang, 1993).

The second fuzzy layer is shown as π, fixed node in Fig. 2. It aids in estimating the value of computing the rules' firing strengths:

$$O_i^2 = \mu_A(C_v)\mu_B(D_{gr})\mu_C(d/R)\mu_D(\lambda) = w_i \quad for \quad i = 1,2,3,4 \tag{10}$$

The third normalization layer labeled N normalizes the firing strengths of the rules:

$$O_i^3 = \frac{w_i}{w_1 + w_2 + w_3 + w_4} = \widehat{w}_i \tag{11}$$

The fourth fuzzy inference layer comprises nodes that have the following adaptive node function:

$$O_i^4 = \widehat{w}_i f_i \tag{12}$$

The fifth defuzzification layer has fixed nodes and is indicated by the "∑". It is the result layer of the ANFIS system, which is the sum of all outputs from the fourth layer:

$$O_i^5 = \sum_{i=1}^{2} \widehat{w}_i f_i = \frac{\left(\sum_{i=1}^{2} w_i f_i\right)}{w_1 + w_2 + w_3 + w_4} \tag{13}$$

In the neuro-fuzzy model, there are also nonlinear membership features, leading to a considerable reduction in the cost of implementing a simple design based on rules and memory usage. This approach is used to evaluate the efficiency of nonlinear systems with model-defined input and output data sets. ANFIS MFs are optimized with the help of combining least-squares and back-propagation gradient descent methods. During the training run, the parameter is optimized to minimize the error between the output and the target variables.

3.3. The proposed ANFISWCA method

Eskandar et al. (2012a) established the WCA, which is inspired by the hydrological water cycle (Khalilpourazari and Khalilpourazary, 2019; Yavari and Robati, 2021). It optimizes based on rivers, streams, and the sea, with streams flowing into rivers that flow into the sea (Sadollah et al., 2016). Following a rainfall process, variables (streams) are formed at random. Therefore, a condition must be stated to ensure choosing the best stream with the lowest cost function (Adnan et al., 2021a; Eskandar et al., 2012b; Sadollah et al., 2016). The streams, rivers, and sea are then classified as good raindrops based on their performances among the other alternatives.

The sea is picked as the best river, and one excellent raindrop is chosen as the best river. The remaining streams flow either into the rivers or the sea (Sadollah et al., 2016). For an N-dimensional problem, the following expression is used (Sadollah et al., 2016):

$$Raindrop = [x_1, x_2, x_3, \cdots x_N] \tag{14}$$

To begin the optimization, the candidate solution matrix (population of raindrops) is created with dimensions N_{pop}*N_{var}. The X matrix was randomly generated in the variable (N_{var}) and population (N_{pop}) sizes.

$$\begin{aligned}\text{Population of raindrops} &= \begin{bmatrix}\text{Raindrop}_1\\ \text{Raindrop}_2\\ \text{Raindrop}_3\\ \vdots\\ \text{Raindrop}_{N_{\text{pop}}}\end{bmatrix}\\ &= \begin{bmatrix} x_1^1 & x_2^1 & x_3^1 & \cdots & x_{N_{\text{var}}}^1\\ x_1^2 & x_2^2 & x_3^2 & \cdots & x_{N_{\text{var}}}^2\\ \vdots & \vdots & \vdots & \vdots & \vdots\\ x_1^{N_{\text{pop}}} & x_2^{N_{\text{pop}}} & x_3^{N_{\text{pop}}} & \cdots & x_{N_{\text{var}}}^{N_{\text{pop}}}\end{bmatrix}\end{aligned} \tag{15}$$

To calculate the cost of a raindrop, the algorithm uses the cost function (C):

$$C_i = \text{Cost}_i = f\left(x_1^i, x_2^i, \ldots, x_{N_{\text{var}}}^i\right) \quad i = 1,2,3,\ldots,N_{\text{pop}} \tag{16}$$

Raindrops are evaluated based on how well they fit the requirements. The first place goes to the river with the lowest cost function. N_{sr} is equal to the product of the number of rivers and a single sea as specified in Equation (17). Equation (18) is used to estimate the rest of the population (raindrops from streams that flow into rivers or the sea).

$$N_{\text{sr}} = \text{Number of Rivers} + \underbrace{1}_{\text{Sea}} \tag{17}$$

$$N_{\text{Raindrops}} = N_{\text{pop}} - N_{\text{sr}} \tag{18}$$

The following formula determines how many streams flow into rivers

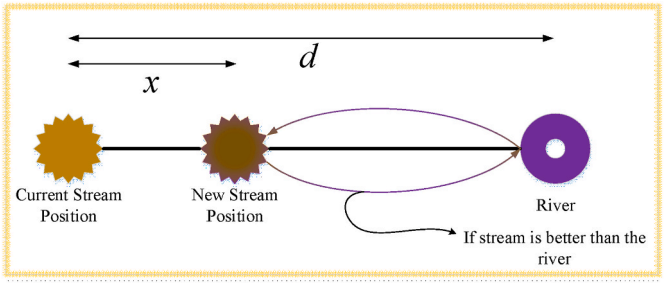

Fig. 3. Architecture of the WCA algorithm.

Table 4
Basic parameters of the WCA.

WCA parameter	Value
Sum of rivers and sea	4
Evaporation condition constant	$1e^{-5}$
Maximum iteration	100
Population	5
Search range	[-1 1]

and the sea:

$$NS_n = round\left\{\left|\frac{Cos\ t_n}{\sum_{i=1}^{N_{sr}} Cos\ t_i}\right| \times N_{Streams}\right\}, i = 1, 2, 3, \cdots, N_{sr} \tag{19}$$

where, NS_n is the total number of streams.

The following equations determine the movement of streams and rivers (Nasir et al., 2020):

$$\overrightarrow{X}_{Stream}(t+1) = \overrightarrow{X}_{Stream}(t) + rand \times C \times \left(\overrightarrow{X}_{Sea}(t) - \overrightarrow{X}_{Stream}(t)\right), \tag{20}$$

$$\overrightarrow{X}_{Stream}(t+1) = \overrightarrow{X}_{Stream}(t) + rand \times C \times \left(\overrightarrow{X}_{River}(t) - \overrightarrow{X}_{Stream}(t)\right), \tag{21}$$

$$\overrightarrow{X}_{River}(t+1) = \overrightarrow{X}_{River}(t) + rand \times C \times \left(\overrightarrow{X}_{Sea}(t) - \overrightarrow{X}_{River}(t)\right), \tag{22}$$

$$X \in (0, C \times d), C > 1 \tag{23}$$

where, *rand* and *C* are important constant values, ranging between [0–1] and [1–2], respectively. Meanwhile, *d* is the current distance between the stream and the river.

As rivers and streams run to the sea, the seawater evaporates. To prevent getting trapped in a local optimum, this assumption is made. The d_{max} would have to steadily decrease over the optimization cycle. To identify whether the river runs into the sea (Fig. 3), the following condition is used:

$$if \left\| \overrightarrow{X}_{Sea}^{t} - \overrightarrow{X}_{River_j}^{t} \right\| < d_{\max} orrand < 0.1 \quad j = 1, 2, 3, \cdots..N_{sr} - 1 \tag{24}$$

$$d_{\max}(t+1) = d_{\max}(t) - \frac{d_{\max}(t)}{It_{\max}}, t = 1, 2, 3, \cdots, It_{\max} \tag{25}$$

Where, d_{max} controls the "intensification level" near the sea. It_{max} is the maximum number of iterations. Eq. (26) contributes to create a new position for the streams:

$$\overrightarrow{X}_{Stream}^{New}(t+1) = \overrightarrow{LB} + rand \times \left(\overrightarrow{UB} - \overrightarrow{LB}\right) \tag{26}$$

Where, *LB* and *UB* are the lower and upper bounds. To hybridize, ANFIS membership functions were optimized in the training phase. In the WCA algorithm, the fitness function was chosen as RMSE. Table 4 depicts the initial parameters of the WCA algorithm.

3.4. Criteria for performance assessment

Four assessment criteria are used to evaluate the performance of the applied models (Equations (27-30); determination coefficient (R^2), root mean square error (*RMSE*), mean absolute error (*MAE*), and variance accounted for (VAF).

$$R^2 = 1 - \frac{\sum_{i=1}^{N}\left(SRI_{i(observed)} - SRI_{i(model)}\right)}{\sum_{i=1}^{N}\left(SRI_{i(observed)} - SRI_{mean}\right)} \tag{27}$$

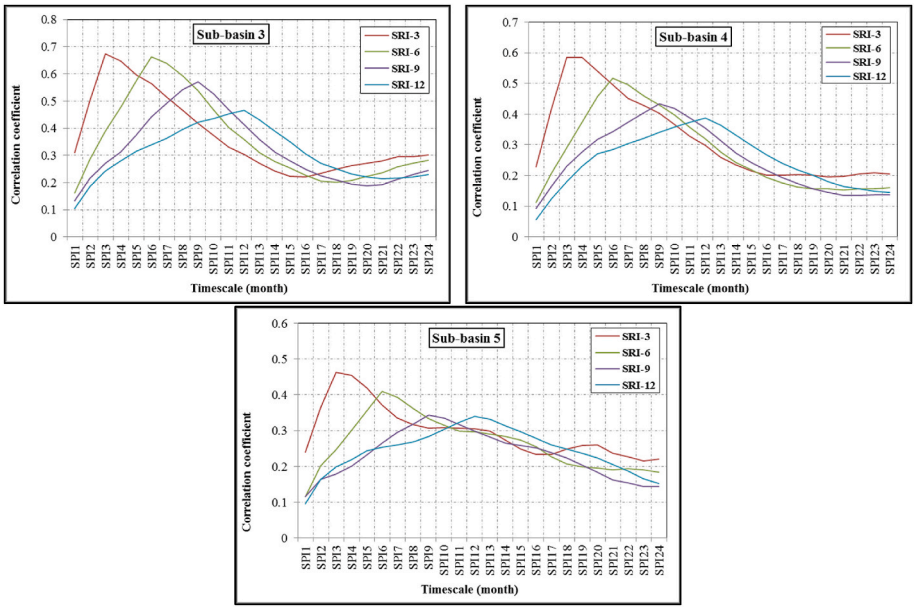

Fig. 4. Correlation between SPI and SRI at different timescales for the sub-basins of the Wadi Mina basin.

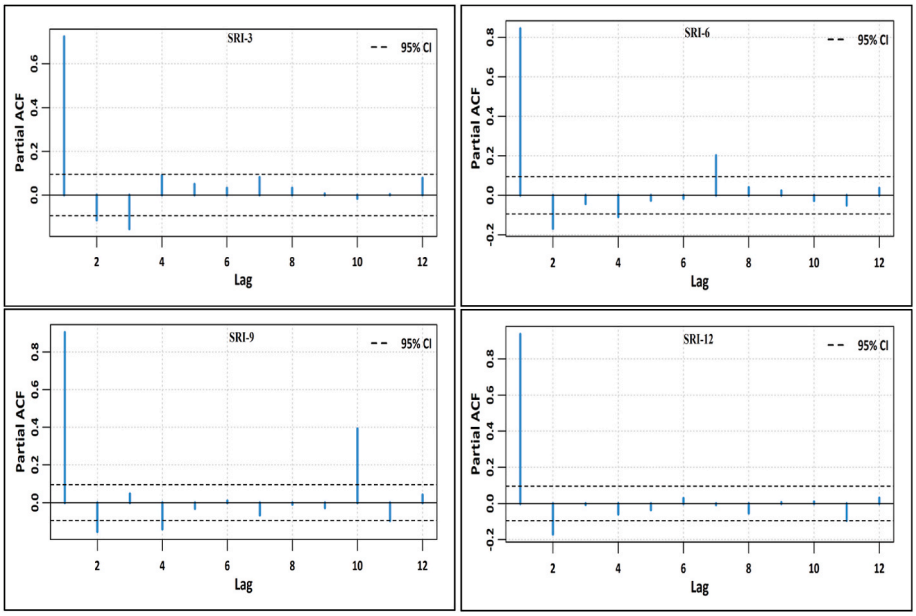

Fig. 5. Partial autocorrelation function for SRI at various time scales (3, 6, 9, 12 months).

Table 5
Input and target variables for SRI forecasting.

Sub-basins	Input variables	Target variable
SB1	SPI-3, SRI-$3_{(t-1)}$, SRI-$3_{(t-2)}$, SRI-$3_{(t-3)}$	SRI-3
	SPI-6, SRI-$6_{(t-1)}$, SRI-$6_{(t-2)}$, SRI-$6_{(t-4)}$, SRI-$6_{(t-7)}$	SRI-6
	SPI-9, SRI-$9_{(t-1)}$, SRI-$9_{(t-2)}$, SRI-$9_{(t-4)}$, SRI-$9_{(t-10)}$, SRI-$9_{(t-11)}$	SRI-9
	SPI-12, SRI-$12_{(t-1)}$, SRI-$12_{(t-11)}$	SRI-12
SB2	SPI-3, SRI-$3_{(t-1)}$, SRI-$3_{(t-4)}$	SRI-3
	SPI-6, SRI-$6_{(t-1)}$, SRI-$6_{(t-2)}$, SRI-$6_{(t-7)}$	SRI-6
	SPI-9, SRI-$9_{(t-1)}$, SRI-$9_{(t-10)}$, SRI-$9_{(t-11)}$	SRI-9
	SPI-12, SRI-$12_{(t-1)}$	SRI-12
SB3	SPI-3, SRI-$3_{(t-1)}$, SRI-$3_{(t-2)}$, SRI-$3_{(t-3)}$, SRI-$3_{(t-4)}$	SRI-3
	SPI-6, SRI-$6_{(t-1)}$, SRI-$6_{(t-2)}$, SRI-6(t-3), SRI-$6_{(t-4)}$, SRI-$6_{(t-5)}$, SRI-$6_{(t-7)}$	SRI-6
	SPI-9, SRI-$9_{(t-1)}$, SRI-$9_{(t-2)}$, SRI-$9_{(t-10)}$	SRI-9
	SPI-12, SRI-$12_{(t-1)}$, SRI-$12_{(t-2)}$, SRI-$12_{(t-8)}$	SRI-12
SB4	SPI-3, SRI-$3_{(t-1)}$, SRI-$3_{(t-2)}$, SRI-$3_{(t-3)}$, SRI-$3_{(t-4)}$	SRI-3
	SPI-6, SRI-$6_{(t-1)}$, SRI-$6_{(t-2)}$, SRI-$6_{(t-7)}$	SRI-6
	SPI-9, SRI-$9_{(t-1)}$, SRI-$9_{(t-2)}$, SRI-$9_{(t-10)}$	SRI-9
	SPI-12, SRI-$12_{(t-1)}$, SRI-$12_{(t-2)}$, SRI-$12_{(t-11)}$	SRI-12
SB5	SPI-3, SRI-$3_{(t-1)}$, SRI-$3_{(t-2)}$, SRI-$3_{(t-3)}$, SRI-$3_{(t-4)}$, SRI-$3_{(t-7)}$, SRI-$3_{(t-9)}$	SRI-3
	SPI-6, SRI-$6_{(t-1)}$, SRI-$6_{(t-7)}$	SRI-6
	SPI-9, SRI-$9_{(t-1)}$, SRI-$9_{(t-2)}$, SRI-$9_{(t-10)}$	SRI-9
	SPI-12, SRI-$12_{(t-1)}$, SRI-$12_{(t-2)}$, SRI-$12_{(t-6)}$, SRI-$12_{(t-7)}$, SRI-$12_{(t-8)}$	SRI-12

$$RMSE = \sqrt{\frac{1}{N}\sum_{i=1}^{N}\left(SRI_{i(observed)} - SRI_{i(model)}\right)} \quad (28)$$

$$MAE = \frac{1}{N}\sum_{i=1}^{N}\left|\left(SRI_{ti(observed)} - SRI_{ti(model)}\right)\right| \quad (29)$$

$$VAF = \left[1 - \frac{\sum_{i=1}^{N}\left(SRI_{i(observed)} - SRI_{i(model)}\right)^2}{\sum_{i=1}^{N}\left(SRI_{i(observed)} - \overline{SRI_{i(observed)}}\right)^2}\right] \quad (30)$$

Where, N is the number of records, $SRI_{i(observed)}$ and $SRI_{i(model)}$ are the actual and forecasted SRI, respectively, and SRI_{mean} is the mean actual SRI.

4. Result and discussion

4.1. Selection of input variables

SPI was calculated as a meteorological drought index on various timescales (1–24 months), and the hydrological-based drought index (namely SRI) was calculated over three, six, nine-, and twelve-month timescales. As shown in Fig. 4, a correlation analysis was done between SPI (1–24 months timescale) and SRI at 3-, 6-, 9- and 12- month, timescales. As input for SRI predicting at 3-, 6-, 9-, and 12-month timescales, the SPI timeline that best reacts to SRI-3, -6, -9, and 12-months was selected. In addition, the ideal inputs (lags) for all SRI periods were determined using the partial autocorrelation function (PACF) at a 5% significance level, as illustrated in Fig. 5. In these graphs, the brown dashed lines show the upper and lower critical limits at a significance level of 5%. Machine learning models can use statistically significant delays where the PACF value exceeds the bounds as input. Table 5 shows the optimum input configuration for SRI prediction that was employed in this study. Here, as an indication, we present only the graphs concerning sub-basin 1 (Figs. 5 and 6).

Fig. 4 shows the SPI and SRI correlations for 5 different sub-basins. For all sub-basins, SPI and SRI have a better correlation on the short timescale. In higher accumulation periods, the number of dry months increases and therefore precipitation has a lower contribution to streamflow. Accordingly, correlation between SPI and SRI decreases at higher time scales. The SPI and SRI values at different timescales formed almost similar correlations in sub-basins. Especially for sub-basin 2, the correlation differences in the timescales were observed more clearly. Almost the same correlation was observed for sub-basin 1 and 5 for the 6 and 9-month scales. The worst correlations for SRI 3, 6, 9, and 12 are for the lower scales of the SPI timescales, respectively. The correlations values tend to decrease after the 13-month scale for all sub-basins. The best correlations were obtained for sub-basin 1.

Fig. 5 indicates the most significant lag correlations for the 3, 6, 9, and 12-timescales of the SRI index, respectively for sub-basin 1. Since there is no "rule of thumb" for recognizing relevant inputs (Adamowski, 2008), we used PACF to determine optimal runoff lags and to calculate

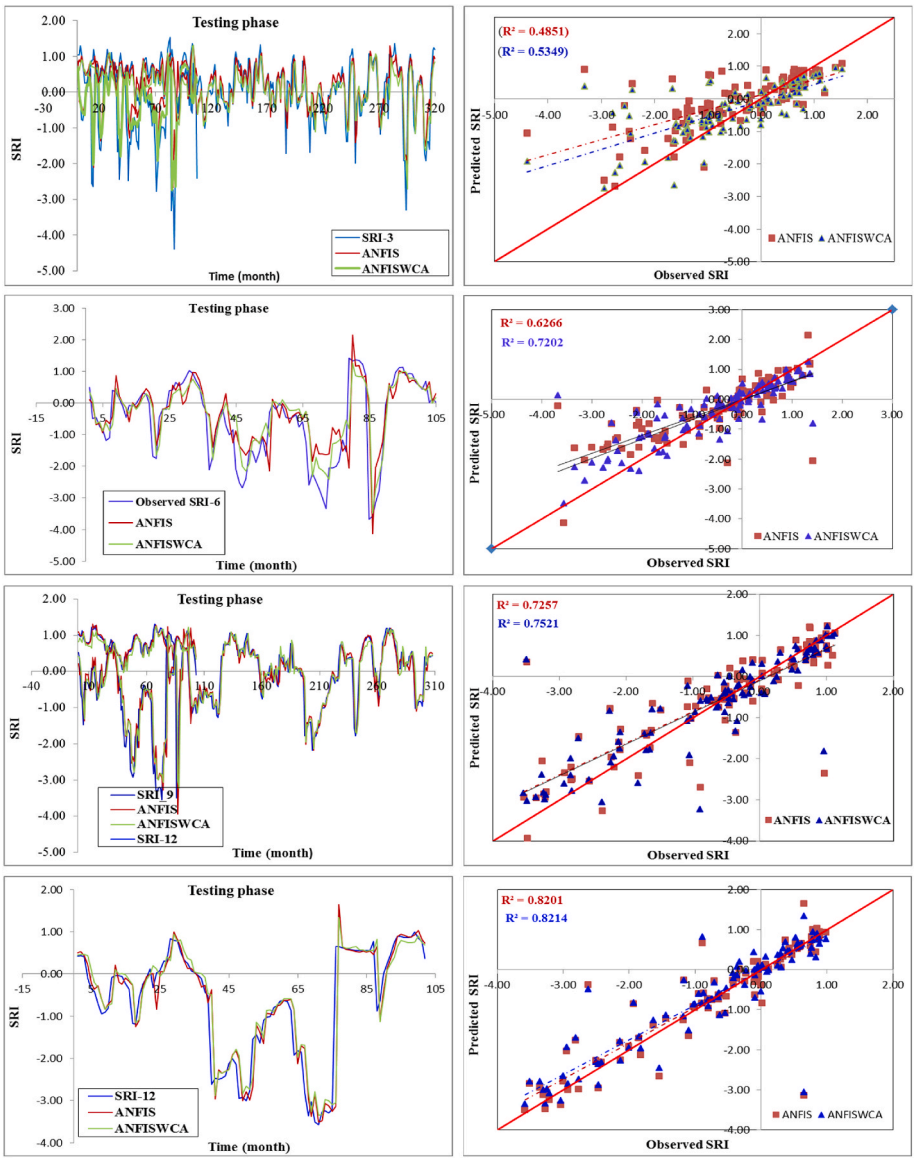

Fig. 6. Comparison between predicted and observed SRI (3-, 6-, 9-, and 12- timescale) values by ANFIS and ANFISWCA while testing phase at sub-basin 1.

the SRI index (Deo et al., 2017; Sudheer et al., 2002; Tiwari and Chatterjee, 2011). The 95% confidence bounds were calculated using these lag values. There was the greatest correlation between *t*-1 lag and all other timescales. In the 9-month timeframe, SRI showed a significant correlation of *t*-10 lag. The statistical method tried to extract lagging information from the signal to analyze time intervals that existed between the current and the past indices. Based on the correlation (R) between the lagged combination coefficients, the optimal inputs were determined for each time lag.

4.2. *Inter-comparison between models for SRI prediction*

In this study, ANFIS as the base model and novel hybridized ANFISWCA were applied to predict SRI in five sub-basins. All model results are shown in Table 6 and Table 7 for the training and testing phases, respectively. The data was split into training (70%) and testing (30%) stages. Table 6 presents the performance of both models in all the sub-basins and at all SRI timescales during the training phase. Results showed that the performance of SRI-12 in comparison to other SRI timescales in all sub-basins is best.

Table 7 represents the results of the performance for all cases in the testing phase. Results indicated that hybridized ANFISWCA was superior to standalone ANFIS for almost all cases. Hybridized ANFISWCA achieved a maximum of 29.6% and 37.38% improvement according to RMSE and MAE in SB2 at SRI-12 for the testing phase. When all cases are examined, the best performance occurred in SB4 at the 12-month timescale (SRI-12) with RMSE = 0.377. When comparing the sub-basins, the best model performance was obtained at SRI-12 for ANFISWCA and SB4.

Over/Under-fitting is an important problem to be considered for modeling studies. Over-fitting means that the model performs much better in the training phase than in the testing phase, while under-fitting is the opposite. The most consistent model is when the training and testing performances are closer to each other. According to the training and testing stages, it was observed that the ANFIS model caused over-fitting problems. In particular, SRI-12 in SB2 had RMSE = 0.18 and RMSE = 0.599 in the training and testing phase with ANFIS. For all cases, ANFISWCA prevented over/under-fitting issues, thus providing more reliable modeling. The results revealed that ANFISWCA significantly reduced the scattering of the models and was partially successful in improving the correlation. Two important indicators of data scattering are RMSE and MAE, and correlation metrics are R^2 and VAF. It can

Table 6
Model results for different sub-basins and timescales in the training phase.

Sub-basins	Timescale	ANFIS				ANFISWCA			
		R^2	RMSE	MAE	VAF	R^2	RMSE	MAE	VAF
SB1	SRI-3	0.709	0.379	0.273	70.920	0.637	0.445	0.331	63.659
	SRI-6	0.795	0.355	0.244	79.502	0.739	0.403	0.272	73.914
	SRI-9	0.897	0.246	0.174	89.661	0.858	0.289	0.188	85.797
	SRI-12	0.924	0.210	0.143	92.402	0.881	0.263	0.182	88.108
SB2	SRI-3	0.736	0.361	0.258	73.618	0.684	0.410	0.301	68.444
	SRI-6	0.862	0.263	0.177	86.239	0.805	0.340	0.250	80.306
	SRI-9	0.926	0.190	0.126	92.647	0.888	0.234	0.144	88.805
	SRI-12	0.935	0.180	0.107	93.486	0.921	0.200	0.112	92.058
SB3	SRI-3	0.812	0.431	0.330	81.167	0.717	0.547	0.399	69.589
	SRI-6	0.850	0.381	0.246	84.972	0.782	0.461	0.297	78.179
	SRI-9	0.885	0.330	0.225	88.482	0.799	0.437	0.262	79.907
	SRI-12	0.908	0.289	0.193	90.819	0.852	0.369	0.237	85.100
SB4	SRI-3	0.693	0.496	0.352	69.341	0.538	0.621	0.426	53.370
	SRI-6	0.773	0.466	0.328	77.255	0.719	0.518	0.344	71.871
	SRI-9	0.875	0.343	0.234	87.486	0.842	0.386	0.250	84.147
	SRI-12	0.900	0.304	0.202	89.998	0.845	0.378	0.247	84.524
SB5	SRI-3	0.775	0.430	0.313	77.456	0.673	0.518	0.363	67.230
	SRI-6	0.872	0.329	0.235	87.238	0.814	0.404	0.268	80.864
	SRI-9	0.919	0.263	0.179	91.869	0.907	0.281	0.183	90.695
	SRI-12	0.967	0.166	0.115	96.730	0.944	0.218	0.133	94.402

Table 7
Model results for different sub-basins and timescales in the testing phase.

Sub-basins	Timescale	ANFIS				ANFISWCA			
		R^2	RMSE	MAE	VAF	R^2	RMSE	MAE	VAF
SB1	SRI-3	0.485	0.916	0.606	48.358	0.535	0.815	0.533	53.190
	SRI-6	0.627	0.796	0.516	62.522	0.720	0.691	0.439	71.278
	SRI-9	0.725	0.698	0.424	72.273	0.752	0.660	0.374	75.144
	SRI-12	0.820	0.571	0.288	81.304	0.822	0.566	0.304	81.896
SB2	SRI-3	0.602	0.710	0.564	60.014	0.634	0.637	0.484	62.604
	SRI-6	0.813	0.544	0.409	80.506	0.810	0.526	0.386	79.996
	SPI-9	0.717	0.602	0.410	71.371	0.755	0.561	0.343	75.425
	SRI-12	0.816	0.599	0.420	76.782	0.848	0.422	0.263	84.795
SB3	SRI-3	0.641	0.615	0.459	63.741	0.645	0.619	0.466	63.519
	SRI-6	0.657	0.606	0.423	65.370	0.695	0.571	0.383	69.520
	SRI-9	0.661	0.624	0.396	62.845	0.687	0.572	0.337	68.162
	SRI-12	0.721	0.525	0.338	71.621	0.741	0.503	0.295	73.771
SB4	SRI-3	0.680	0.640	0.477	67.902	0.758	0.563	0.420	70.656
	SRI-6	0.807	0.477	0.349	80.569	0.842	0.457	0.335	83.310
	SRI-9	0.889	0.383	0.259	87.195	0.894	0.367	0.250	89.341
	SRI-12	0.886	0.414	0.293	88.336	0.881	0.377	0.234	87.926
SB5	SRI-3	0.509	0.871	0.602	48.525	0.514	0.847	0.618	51.353
	SRI-6	0.567	0.741	0.487	56.284	0.649	0.668	0.403	64.885
	SRI-9	0.760	0.533	0.320	74.903	0.766	0.519	0.302	76.045
	SRI-12	0.733	0.525	0.312	70.786	0.794	0.463	0.252	76.974

be said that the minimization of scattering in the hybridization process is the use of RMSE as a fitness function.

On the other hand, over/under-estimation is an important problem that indicates how far the model deviates from its observed values. The scatterplot of observed and computed SRI for ANFIS and ANFISWCA is shown in Figs. 6 and 7 for both the testing and training stages. Results indicated that the predicted SRI for the proposed method (ANFISWCA) corresponds well with their measured counterparts, with the results remaining approximately on the bisector line with a slight scatter. It was observed that extreme drought and wetness values were modeled more accurately with ANFISWCA. The proposed method, ANFISWCA provided a better generalization of the data.

It is crucial to consider the implications of the enhanced performance of the ANFISWCA model for drought forecasting and water resource management in semi-arid regions. Our results showcase the potential of hybridized models, such as ANFISWCA, to deliver more accurate and reliable predictions for water resource management, ultimately resulting in improved decision-making and increased resilience in these vulnerable areas. Adnan et al. (2021a) demonstrated that ANFISWCA outperforms other methods in drought modeling for humid regions. Furthermore, it is evident that the hybridized ANFISWCA model can significantly contribute to the field of drought forecasting and water resource management. This contribution is particularly vital for semi-arid regions, where precise prediction of water resources and droughts is essential for sustainable development and the well-being of local communities. By further refining and optimizing the ANFISWCA model, researchers can continue to advance the understanding and prediction of water resources in these regions, ultimately leading to more effective resource management and adaptation strategies.

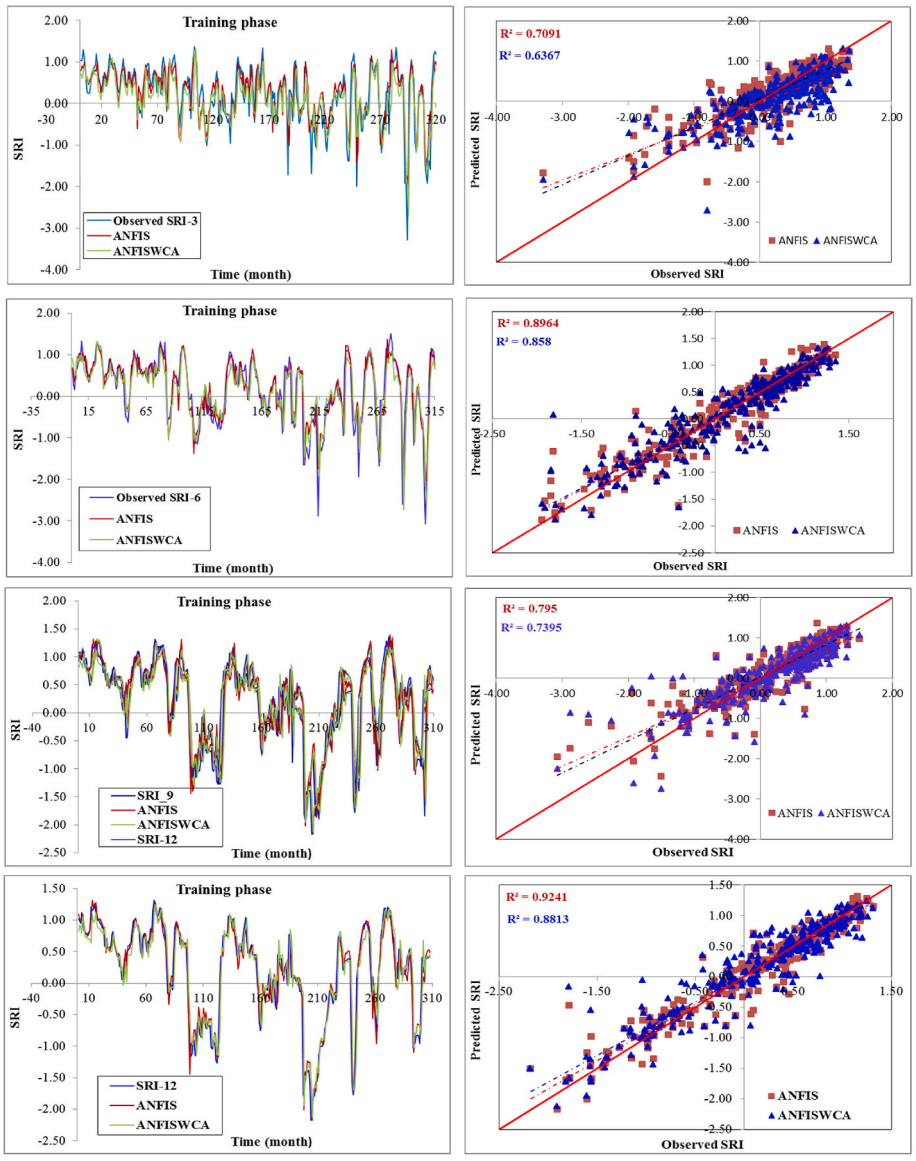

Fig. 7. Comparison between predicted and observed SRI (3-, 6-, 9-, and 12- timescale) values by ANFIS and ANFISWCA while training phase at sub-basin 1.

5. Conclusions

Water quality and quantity, environmental management, agricultural products, and food security are all negatively impacted by drought. Therefore, drought remains one of the most challenging natural phenomena to predict due to its complexity. A variety of factors at different temporal and geographical scales affect drought severity and frequency. Drought modeling has received attention in the application of artificial intelligence techniques to build reliable approaches with high computing capabilities during the last ten years. In this context, this research used the conventional ANFIS and suggested hybrid ANFISWCA models to anticipate hydrological drought in northwest Algeria. Several statistical metrics were utilized to evaluate the standalone and hybrid models, including: R^2, RMSE, MAE, and VAF. The major findings of this study are listed as follows:

- Employing WCA improved the accuracy of the standalone model.
- The ANFISWCA model was associated with better evaluation metrics compared to the ANFIS model for modeling SRI-3 during the testing phase.
- The same implications apply to modeling SRI-6 and SRI-9 drought measures.
- The ANFISWCA model was shown to be the most reliable model for modeling SRI-12.

The proposed hybrid technique showed a higher ability for controlling the complex dynamics of drought at different timescales. Our study was limited to the use of historical SPI and SRI series to predict hydrological drought onset. Inasmuch as evaporation is an important parameter in streamflow variation in arid and semiarid regions, further studies could employ the proposed hybrid algorithm for hydrological drought forecasting using standardized precipitation and evaporation index that may better represent streamflow variations at dry seasons. The proposed model could also be used to develop a robust intelligent system for forecasting and mapping agricultural drought at multi-timescales, assisting in sustainable water resources management, and determining remedial techniques for coping with drought at study area.

CRediT authorship contribution statement

Conceptualization: M.A. and B.M.; methodology: E.G. and A.D.M.;

software: E.G., M.J., and A.D.M; validation, M.A., E.G., A.D.M., N. E., and M.J.; visualization: M.A., and M.J.; formal analysis: M.A. and N.E.; investigation: M.A., N.E., E.G., M.J., B.M., and A.D.M.; writing—original draft: M.A., N.E., E.G., M.J., and A.D.M.; writing—review and editing: M.A., N.E., E.G., M.J., B.M. and A.D.M.; supervision, M.A., E.G., N.E., M. J., and A.D.M

Funding

Open access funding provided by Lund University.

Declaration of competing interest

The authors declare that they have no known competing financial interests or personal relationships that could have appeared to influence the work reported in this paper.

Data availability

Data will be made available on request.

Acknowledgments

The authors would like thanks the Algerian General Directorate of Scientific Research and Technological Development (DGRSDT) and the ANRH agency for proving the dataset for the current research.

References

Achite, M., Banadkooki, F.B., Ehteram, M., Bouharira, A., Ahmed, A.N., Elshafie, A., 2022a. Exploring Bayesian model averaging with multiple ANNs for meteorological drought forecasts. Stoch. Environ. Res. Risk Assess. 36, 1835–1860. https://doi.org/10.1007/S00477-021-02150-6/METRICS.

Achite, M., Jehanzaib, M., Elshaboury, N., Kim, T.W., 2022b. Evaluation of machine learning techniques for hydrological drought modeling: a case study of the Wadi Ouahrane Basin in Algeria. Water 14, 431. https://doi.org/10.3390/W14030431, 2022.

Achite, M., Touaibia, B., 2007. Sécheresse et gestion des ressources en eau dans le bassin versant de la Mina. In: Algérie. 2ème Colloque International Sur L'eau et L'Environnement. Available online: www.worldwatercouncil.org. (Accessed 5 September 2021).

Adamowski, J.F., 2008. Development of a short-term river flood forecasting method for snowmelt driven floods based on wavelet and cross-wavelet analysis. J. Hydrol. (Amst.) 353, 247–266. https://doi.org/10.1016/J.JHYDROL.2008.02.013.

Adnan, R.M., Mostafa, R., Islam, A.R.M.T., Kisi, O., Kuriqi, A., Heddam, S., 2021a. Estimating reference evapotranspiration using hybrid adaptive fuzzy inferencing coupled with heuristic algorithms. Comput. Electron. Agric. 191, 106541 https://doi.org/10.1016/J.COMPAG.2021.106541.

Adnan, R.M., Mostafa, R.R., Islam, A.R.M.T., Gorgij, A.D., Kuriqi, A., Kisi, O., 2021b. Improving drought modeling using hybrid random vector functional link methods. Water (Switzerland) 13, 3379. https://doi.org/10.3390/W13233379/S1.

AghaKouchak, A., 2014. A baseline probabilistic drought forecasting framework using standardized soil moisture index: application to the 2012 United States drought. Hydrol. Earth Syst. Sci. 18, 2485–2492. https://doi.org/10.5194/HESS-18-2485-2014.

Ahmadalipour, A., Moradkhani, H., Demirel, M.C., 2017. A comparative assessment of projected meteorological and hydrological droughts: elucidating the role of temperature. J. Hydrol. (Amst.) 553, 785–797. https://doi.org/10.1016/J.JHYDROL.2017.08.047.

Awange, J.L., Mpelasoka, F., Goncalves, R.M., 2016. When every drop counts: analysis of Droughts in Brazil for the 1901-2013 period. Sci. Total Environ. 566–567, 1472–1488. https://doi.org/10.1016/J.SCITOTENV.2016.06.031.

Azizi, E., Tavakoli, M., Karimi, H., Faramarzi, M., 2019. Evaluating the efficiency of the neural network to other methods in predicting drought in arid and semi-arid regions of western Iran. Arabian J. Geosci. 12, 1–16. https://doi.org/10.1007/S12517-019-4654-Z.

Başakın, E.E., Ekmekcioğlu, Ö., Özger, M., 2021. Drought prediction using hybrid soft-computing methods for semi-arid region. Model Earth Syst. Environ. 7, 2363–2371. https://doi.org/10.1007/S40808-020-01010-6/METRICS.

Belayneh, A., Adamowski, J., Khalil, B., Quilty, J., 2016. Coupling machine learning methods with wavelet transforms and the bootstrap and boosting ensemble approaches for drought prediction. Atmos. Res. 172–173, 37–47. https://doi.org/10.1016/J.ATMOSRES.2015.12.017.

Bhalme, H.N., Mooley, D.A., 1980. Large-scale droughts/floods and monsoon circulation. Mon. Weather Rev. 108, 1197–1211.

Danandeh Mehr, A., Jafar, M., Safari, S., Nourani, V., 2021. Wavelet packet-genetic programming: a new model for meteorological drought hindcasting. Tek. Dergi 32, 11029–11050. https://doi.org/10.18400/TEKDERG.605453.

Danandeh Mehr, A., Vaheddoost, B., Mohammadi, B., 2020. ENN-SA: a novel neuro-annealing model for multi-station drought prediction. Comput. Geosci. 145, 104622 https://doi.org/10.1016/j.cageo.2020.104622.

Deo, R.C., Tiwari, M.K., Adamowski, J.F., Quilty, J.M., 2017. Forecasting effective drought index using a wavelet extreme learning machine (W-ELM) model. Stoch. Environ. Res. Risk Assess. 31 https://doi.org/10.1007/s00477-016-1265-z.

Doshi, S.C., Shanmugam, M.S., Akib, S., 2022. Assessment of artificial neural network through drought indices. Eng 2023 4, 31–46. https://doi.org/10.3390/ENG4010003.

Emamgholizadeh, S., Mohammadi, B., 2021. New hybrid nature-based algorithm to integration support vector machine for prediction of soil cation exchange capacity. Soft Comput. 25 https://doi.org/10.1007/s00500-021-06095-4.

Eskandar, H., Sadollah, A., Bahreininejad, A., Hamdi, M., 2012a. Water cycle algorithm – a novel metaheuristic optimization method for solving constrained engineering optimization problems. Comput. Struct. 110–111, 151–166. https://doi.org/10.1016/J.COMPSTRUC.2012.07.010.

Eskandar, H., Sadollah, A., Bahreininejad, A., Hamdi, M., 2012b. Water cycle algorithm - a novel metaheuristic optimization method for solving constrained engineering optimization problems. Comput. Struct. 110–111. https://doi.org/10.1016/j.compstruc.2012.07.010.

Gholizadeh, R., Yılmaz, H., Danandeh Mehr, A., 2022. Multitemporal meteorological drought forecasting using Bat-ELM. Acta Geophysica 70, 917–927. https://doi.org/10.1007/S11600-022-00739-1/METRICS.

Habibi, B., Meddi, M., Torfs, P.J.J.F., Remaoun, M., Van Lanen, H.A.J., 2018. Characterisation and prediction of meteorological drought using stochastic models in the semi-arid Chéliff–Zahrez basin (Algeria). J Hydrol Reg Stud 16, 15–31. https://doi.org/10.1016/J.EJRH.2018.02.005.

Ham, Y.S., Sonu, K.B., Paek, U.S., Om, K.C., Jong, S. Il, Jo, K.R., 2022. Comparison of LSTM network, neural network and support vector regression coupled with wavelet decomposition for drought forecasting in the western area of the DPRK. Nat. Hazards 116, 2619–2643. https://doi.org/10.1007/S11069-022-05781-2/METRICS.

Hanjra, M.A., Qureshi, M.E., 2010. Global water crisis and future food security in an era of climate change. Food Pol. 35, 365–377. https://doi.org/10.1016/J.FOODPOL.2010.05.006.

Hao, Z., AghaKouchak, A., Nakhjiri, N., Farahmand, A., 2014. Global integrated drought monitoring and prediction system. Scientific Data 1 (1 1), 1–10. https://doi.org/10.1038/sdata.2014.1, 2014.

Hao, Z., Singh, V.P., Xia, Y., 2018. Seasonal drought prediction: advances, challenges, and future prospects. Rev. Geophys. 56, 108–141. https://doi.org/10.1002/2016RG000549.

Hosseini-Moghari, S.M., Araghinejad, S., 2015. Monthly and seasonal drought forecasting using statistical neural networks. Environ. Earth Sci. 74, 397–412. https://doi.org/10.1007/S12665-015-4047-X/METRICS.

Jadav, K., Panchal, M., 2012. Optimizing weights of artificial neural networks using genetic algorithms. Int. J. Adv. Res. Comput. Sci. Electron 1, 47–51.

Jang, J.S., 1993. ANFIS: adaptive-network-based fuzzy inference system. IEEE Trans. Syst.s, Man, and Cybernetics 23 (3), 665–685. https://doi.org/10.1109/21.256541.

Jehanzaib, M., Idrees, M.B., Kim, D., 2021. Comprehensive evaluation of machine learning techniques for hydrological drought forecasting probablistic precipitation nowcasting using multi-machine learning architectures based on radar precipitation data view project modelling view project. https://doi.org/10.1061/(ASCE)IR.1943-4774.0001575.

Khalilpourazari, S., Khalilpourazary, S., 2019. An efficient hybrid algorithm based on Water Cycle and Moth-Flame Optimization algorithms for solving numerical and constrained engineering optimization problems. Soft Comput. 23, 1699–1722. https://doi.org/10.1007/S00500-017-2894-Y/METRICS.

Li, J., Wang, Z., Wu, X., Xu, C.Y., Guo, S., Chen, X., 2020. Toward monitoring short-term droughts using a novel daily scale, standardized antecedent precipitation evapotranspiration index. J. Hydrometeorol. 21, 891–908. https://doi.org/10.1175/JHM-D-19-0298.1.

Li, J., Wang, Z., Wu, X., Zscheischler, J., Guo, S., Chen, X., 2021. A standardized index for assessing sub-monthly compound dry and hot conditions with application in China. Hydrol. Earth Syst. Sci. 25, 1587–1601. https://doi.org/10.5194/HESS-25-1587-2021.

Liang, G., Panahi, F., Ahmed, A.N., Ehteram, M., Band, S.S., Elshafie, A., 2021. Predicting municipal solid waste using a coupled artificial neural network with archimedes optimisation algorithm and socioeconomic components. J. Clean. Prod. 315, 128039 https://doi.org/10.1016/J.JCLEPRO.2021.128039.

Malik, A., Kumar, A., Salih, S.Q., Kim, S., Kim, N.W., Yaseen, Z.M., Singh, V.P., 2020. Drought index prediction using advanced fuzzy logic model: regional case study over Kumaon in India. PLoS One 15, e0233280. https://doi.org/10.1371/JOURNAL.PONE.0233280.

Mckee, T.B., Doesken, N.J., Kleist, J., 1993. The relationship of drought frequency and duration to time scales. Eighth Conference on Applied Climatology 17–22.

Mehdizadeh, S., Ahmadi, F., Danandeh Mehr, A., Safari, M.J.S., 2020. Drought modeling using classic time series and hybrid wavelet-gene expression programming models. J. Hydrol. (Amst.) 587, 125017. https://doi.org/10.1016/J.JHYDROL.2020.125017.

Mehran, A., Mazdiyasni, O., AghaKouchak, A., 2015. A hybrid framework for assessing socioeconomic drought: linking climate variability, local resilience, and demand. J. Geophys. Res. 120, 7520–7533. https://doi.org/10.1002/2015JD023147.

Mirboluki, A., Mehraein, M., Kisi, O., 2022. Improving Accuracy of Neuro Fuzzy and Support Vector Regression for Drought Modelling Using Grey Wolf Optimization 67, 1582–1597. https://doi.org/10.1080/02626667.2022.2082877.

Mohammadi, B., 2023. Modeling various drought time scales via a merged artificial neural network with a firefly algorithm. Hydrology 10, 58. https://doi.org/10.3390/HYDROLOGY10030058, 2023.

Moreira, E.E., Coelho, C.A., Paulo, A.A., Pereira, L.S., Mexia, J.T., 2008. SPI-based drought category prediction using loglinear models. J. Hydrol. (Amst.) 354, 116–130. https://doi.org/10.1016/J.JHYDROL.2008.03.002.

Naresh Kumar, M., Murthy, C.S., Sesha sai, M.V.R., Roy, P.S., 2009. On the use of Standardized Precipitation Index (SPI) for drought intensity assessment. Meteorol. Appl. 16, 381–389. https://doi.org/10.1002/MET.136.

Nasir, M., Sadollah, A., Choi, Y.H., Kim, J.H., 2020. A comprehensive review on water cycle algorithm and its applications. Neural Comput. Appl. 32, 17433–17488. https://doi.org/10.1007/S00521-020-05112-1/METRICS.

Palmer, W.C., 1965. Meteorological Drought, 30. US Department of Commerce, Weather Bureau [WWW Document].

Panda, K.C., Singh, R.M., Thakural, L.N., Sahoo, D.P., 2022. Representative grid location-multivariate adaptive regression spline (RGL-MARS) algorithm for downscaling dry and wet season rainfall. J. Hydrol. (Amst.) 605, 127381. https://doi.org/10.1016/J.JHYDROL.2021.127381.

Pande, C.B., Al-Ansari, N., Kushwaha, N.L., Srivastava, A., Noor, R., Kumar, M., Moharir, K.N., Elbeltagi, A., 2022. Forecasting of SPI and meteorological drought based on the artificial neural network and M5P model tree. Land 11, 2040. https://doi.org/10.3390/LAND11112040, 2022.

Rahmouni, A., Meddi, M., Saaed, A.H., 2022. Hydrological drought response to meteorological drought propagation and basin characteristics (case study: northwest of Algeria). Russ. Meteorol. Hydrol. 47, 708–717. https://doi.org/10.3103/S1068373922090096/METRICS.

Rais, M.C., Dekhandji, F.Z., Recioui, A., Rechid, M.S., Djedi, L., 2022. Comparative study of optimization techniques based PID tuning for automatic voltage regulator system. Engineering Proceedings 14, 21. https://doi.org/10.3390/ENGPROC2022014021, 2022.

Ribeiro, A.F.S., Pires, C.A.L., 2016. Seasonal drought predictability in Portugal using statistical–dynamical techniques. Phys. Chem. Earth, Parts A/B/C 94, 155–166. https://doi.org/10.1016/J.PCE.2015.04.003.

Sadollah, A., Eskandar, H., Lee, H.M., Yoo, D.G., Kim, J.H., 2016. Water cycle algorithm: a detailed standard code. SoftwareX 5, 37–43. https://doi.org/10.1016/J.SOFTX.2016.03.001.

Sattar, M.N., Jehanzaib, M., Kim, J.E., Kwon, H.H., Kim, T.W., 2020. Application of the hidden Markov bayesian classifier and propagation concept for probabilistic assessment of meteorological and hydrological droughts in South Korea. Atmosphere 11, 1000. https://doi.org/10.3390/ATMOS11091000, 2020.

Singh, A.K., Kumar, P., Ali, R., Al-Ansari, N., Vishwakarma, D.K., Kushwaha, K.S., Panda, K.C., Sagar, A., Mirzania, E., Elbeltagi, A., Kuriqi, A., Heddam, S., 2022. An integrated statistical-machine learning approach for runoff prediction. Sustainability 14, 8209. https://doi.org/10.3390/SU14138209, 2022.

Singh, R., Kainthola, A., Singh, T.N., 2012. Estimation of elastic constant of rocks using an ANFIS approach. Appl. Soft Comput. 12, 40–45. https://doi.org/10.1016/J.ASOC.2011.09.010.

Singh, V.K., Panda, K.C., Sagar, A., Al-Ansari, N., Duan, H.F., Paramaguru, P.K., Vishwakarma, D.K., Kumar, A., Kumar, D., Kashyap, P.S., Singh, R.M., Elbeltagi, A., 2022. Novel Genetic Algorithm (GA) based hybrid machine learning-pedotransfer Function (ML-PTF) for prediction of spatial pattern of saturated hydraulic conductivity. Eng. Appl. Comput. Fluid Mech. 16, 1082–1099. https://doi.org/10.1080/19942060.2022.2071994/SUPPL_FILE/TCFM_A_2071994_SM4775.DOCX.

Sudheer, K.P., Gosain, A.K., Ramasastri, K.S., 2002. A data-driven algorithm for constructing artificial neural network rainfall-runoff models. Hydrol. Process. 16, 1325–1330. https://doi.org/10.1002/HYP.554.

Tiwari, M.K., Chatterjee, C., 2011. A new wavelet–bootstrap–ANN hybrid model for daily discharge forecasting. J. Hydroinf. 13, 500–519. https://doi.org/10.2166/HYDRO.2010.142.

Vicente-Serrano, S.M., Beguería, S., López-Moreno, J.I., 2010. A multiscalar drought index sensitive to global warming: the standardized precipitation evapotranspiration index. J. Clim. 23, 1696–1718. https://doi.org/10.1175/2009JCLI2909.1.

Yadav, D., Verma, O.P., 2020. Energy optimization of multiple stage evaporator system using water cycle algorithm. Heliyon 6, e04349. https://doi.org/10.1016/J.HELIYON.2020.E04349.

Yaseen, Z.M., Awadh, S.M., Sharafati, A., Shahid, S., 2018. Complementary data-intelligence model for river flow simulation. J. Hydrol. (Amst.) 567, 180–190. https://doi.org/10.1016/J.JHYDROL.2018.10.020.

Yaseen, Z.M., El-shafie, A., Jaafar, O., Afan, H.A., Sayl, K.N., 2015. Artificial intelligence based models for stream-flow forecasting: 2000–2015. J. Hydrol. (Amst.) 530, 829–844. https://doi.org/10.1016/J.JHYDROL.2015.10.038.

Yavari, H.R., Robati, A., 2021. Developing water cycle algorithm for optimal operation in multi-reservoirs hydrologic system. Water Resour. Manag. 35 (8 35), 2281–2303. https://doi.org/10.1007/S11269-021-02781-Y, 2021.

Zargar, A., Sadiq, R., Naser, B., Khan, F.I., 2011. A review of drought indices. Environ. Rev. 19, 333–349. https://doi.org/10.1139/A11-013.